



Effect of Love Wave Propagation on the Equivalent Seismic Bearing Capacity of Shallow Foundations Using 3D Coulomb Failure Mechanism

Ardavan Izadi · Reza Jamshidi Chenari · Sina Javankhshdel ·
Foroogh Hemmati Masouleh

Received: 4 September 2020 / Accepted: 11 January 2022 / Published online: 24 January 2022
© The Author(s), under exclusive licence to Springer Nature Switzerland AG 2022

Abstract The equivalent seismic bearing capacity factor of shallow strip foundations in the presence of pseudo-dynamic earthquake accelerations induced by Love wave propagation have been evaluated by the limit equilibrium method and application of the three-dimensional Coulomb failure mechanism. A parametric study was conducted to evaluate the influences of different geo-material and geometrical conditions, seismic excitation parameters including earthquake coefficient of accelerations, and wavelength of the Love wave on the seismic bearing capacity factor. The results showed that the earthquake acceleration coefficient and the Love wave frequency (wavelength) are the most important parameters affecting the performance of overlying shallow foundations. It was found that the bearing capacity of shallow footing decreases with the increase of earthquake acceleration and Love wavelength. It was further confirmed that increasing the soil cohesion and footing embedment depth would diminish the detrimental impacts of the surface wave interaction with the overlying shallow footings.

Keywords Pseudo dynamic bearing capacity · Love wave · Limit equilibrium method · Coulomb failure mechanism

1 Introduction

Earthquakes, as one of the most recognized tragic natural disasters, are potentially highly destructive and unpredictable. The statistics of human losses and enormous financial casualties induced by earthquakes signify the importance of risk assessment and evaluation of the effect of seismic forces on foundations failure and its corresponding severe damage to superstructures. Hence, the attention of many researchers has been garnered to the problem of seismic bearing capacity of shallow foundations. To this end, proposing novel solutions to mitigate risks and casualties, implementation of more accurate analytical and numerical analysis methods to evaluate the key parameters contributing to the seismic bearing capacity assessment have been targeted accordingly. Furthermore, consideration of more realistic problem conditions involving seismic excitations, soil strength profiles, third dimension effect of the problem, and evaluation of the effects of body and surface waves excitations on foundation failure have been covered.

The simplicity and capability of the pseudo-static scheme of analysis associated with different methods of analysis such as limit equilibrium method (LEM),

A. Izadi · R. Jamshidi Chenari (✉) ·
F. Hemmati Masouleh
Department of Civil Engineering, Faculty of Engineering,
University of Guilan, Rasht, Guilan, Iran
e-mail: Jamshidi_reza@guilan.ac.ir

S. Javankhshdel
Geomechanics Specialist, Rocscience Inc., 54 Saint
Patrick St., Toronto, ON, Canada

bound theorems of limit analysis, stress characteristics as well as numerical analysis to take into account seismic forces make it more favorable than the pseudo-dynamic loading consideration to investigate the seismic bearing capacity of shallow foundations. The study of Meyerhof (1963) is among the first documented uses of the pseudo-static approach to capture the effect of seismic forces on the ultimate limit load of shallow foundations. In these studies, the effects of seismic forces on the soil mass, i.e. inertia forces of the soil media, were neglected and the seismic forces were only applied by an additional inclination angle to the gravity forces of superstructures. However, innumerable numerical and experimental studies showed that seismic forces admittedly have great impacts on the soil properties and inertia of soil mass. Consequently, the ultimate load of the shallow foundations is strongly dependent on the assumption of seismic excitation effects on the soil media.

Over the several recent decades, many researchers studied the problem of seismic bearing capacity of shallow foundations by taking into account pseudo-static earthquake coefficients of acceleration for both superstructures and soil mass by the implementation of different numerical and analytical methods including limit equilibrium, bound theorem of limit analysis, and stress characteristics method. Budhu and Al-Karni (1993), Paolucci and Pecker (1997), Soubra (1999), Kumar and Rao (2002), Askari and Farzaneh (2003), Kumar and Kumar (2003), Choudhury and Rao (2005), Yamamoto (2010), Kumar and Chakraborty (2013), Chakraborty and Kumar (2015), Ghosh and Debnath (2017), Foroutan Kalourazi et al. (2019), Haghsheno et al. (2020), Nouzari et al. (2021), and Izadi et al. (2021) are among many on this problem.

Despite its robustness, the pseudo-static approach is not able to capture the effect of excitation time duration, excitation frequency, and phase differences. By subjecting the entire soil mass to the same value of accelerations, the pseudo-static method essentially assumes the magnitude and phase of the accelerations to be invariant through the soil body. By taking into account the influences of both shear and primary waves, the amplification of seismic excitations, and the period of lateral shaking, the pseudo-dynamic approach was firstly proposed by Steedman and Zeng (1990) and extended by Choudhury and Nimbalkar (2005). Over recent years, the problems of bearing

capacity of shallow foundations (Ghosh 2008; Ghosh and Choudhury 2011; Saha and Ghosh 2015; Zhou et al. 2016; Saha and Ghosh 2017; Kurup and Kolathayar 2018; Izadi et al. 2019b; Pakdel et al. 2021) and stability of retaining walls (Ghosh and Kolathayar 2011; Bellezza 2014, 2015; Pain et al. 2015; Fathipour et al. 2021) in conjunction with different methods of analysis and application of the pseudo-dynamic approach have received considerable attention.

Although numerous studies were reported on the problem of seismic bearing capacity of shallow foundation via different methods of analysis and different assumptions for capturing the effects of the earthquake excitation, there seem to be little if any published evidence on the influence of the Love wave propagation on foundation failure. Moreover, an additional difficulty arises from the fact that the Love wave velocity is frequency-dependent in nature.

In this study, the limit equilibrium method (LEM) associated with the 3D Coulomb failure mechanism is used to investigate the influence of the Love wave propagation on the seismic bearing capacity of shallow footings. Despite all the other studies on the effects of wave propagation on bearing capacity, the problem under consideration is assumed to be 3D. In fact, the body and surface waves propagate in any arbitrary direction and the bearing capacity of shallow footings strongly depends on the ratio of the wavelength to the dimensions of the foundation. Furthermore, the Love wave cycles along the footing length/width and exerts excitations transversely. To overcome these concerns, the 3D Coulomb failure mechanism was adopted and the most critical case, the direction of the Love wave along the footing length and particle's oscillation perpendicular to the train of Love wave, was considered.

2 Love Wave Propagation

Body waves including primary and shear waves as well as Rayleigh waves propagate through homogeneous elastic half-space. For a soil profile consisting of at least a semi-infinite medium and a soil layer, primary and shear waves may be reflected and partly transmitted through the shared interfaces between the layers. In this case, the successive reflections of SH waves from the interface of the thin soft layer and the

semi-infinite stiffer soil as shown in Fig. 1a may lead to generate Love wave (Kramer 1996; Verruijt 2010). In other words, the necessary condition to observe Love waves is that a low-velocity layer is underlain by a high-velocity half-space. The Love waves are indeed resultant of interference of shear waves in the surficial layer and are often described as SH-waves trapped in the surface layer.

The particle motion of a Love wave, representing a transverse wave, is a side-to-side (back and forth) motion perpendicular to the main direction of the wave propagation without either vertical or longitudinal components as shown in Fig. 1b (Love 1927). In geotechnical earthquake engineering and seismology, the Love waves are known as surface seismic waves that cause horizontal shifting of the surface ground during the action of an earthquake dispersing as a long train of waves to the substantial distances from the source. As the amplitude of Love waves decays more slowly than body waves, these waves lead to strong ground motion and consequently to strong seismic

motions even for earthquakes originated from distant sources (Shearer 2009).

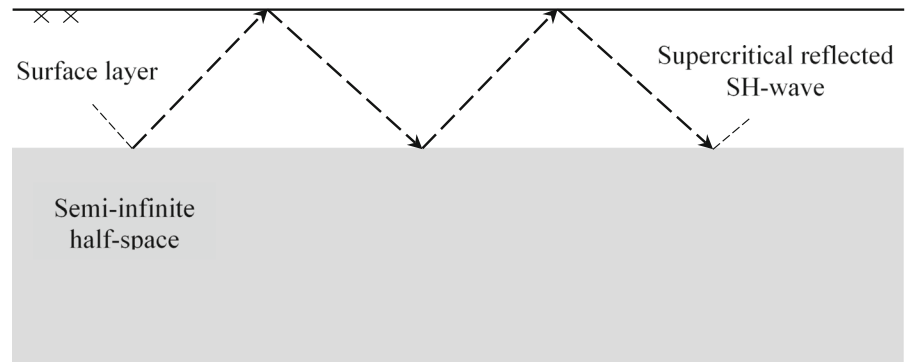
For a surficial layer of thickness H , shear modulus of G_1 and density of ρ_1 overlying a homogenous half-space with shear modulus and density of G_2 and ρ_2 , respectively, as shown in Fig. 2, the love wave travels in the $+x$ direction with the particles oscillating in the $\pm y$ directions, perpendicular to the plane of wave propagation ($x-z$). The particle displacement can then be described as the basic form of Eq. (1).

$$v(x, z, t) = V(z)e^{i(k_1x - \omega t)} \tag{1}$$

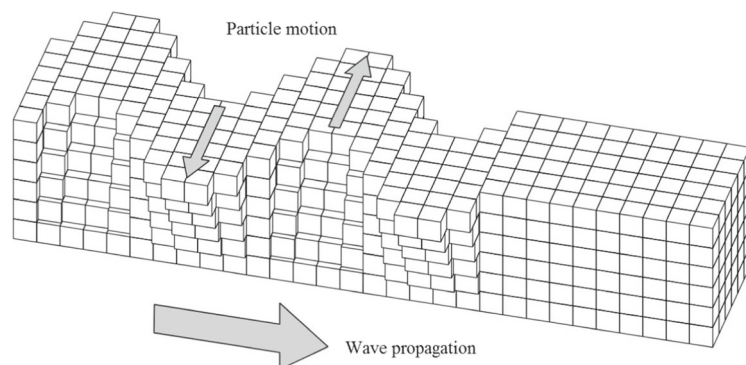
where v is the particle displacement in the y -direction, $V(z)$ is the amplitude describing the variation of the particle displacement with depth, k_1 is the Love wave number, ω is the angular frequency and t is the time of vibration (Kramer 1996).

Note that the third dimension of the failure surface is formed in the out-of-plane direction and the footing length, as illustrated schematically in Fig. 2, is assumed sufficiently long to assure plane strain condition in the out-of-plane direction. Therefore,

Fig. 1 a Generation of the Love wave by successive reflections of SH-wave in a surficial layer, b Love wave propagation and generated transverse particle motion



(a)



(b)

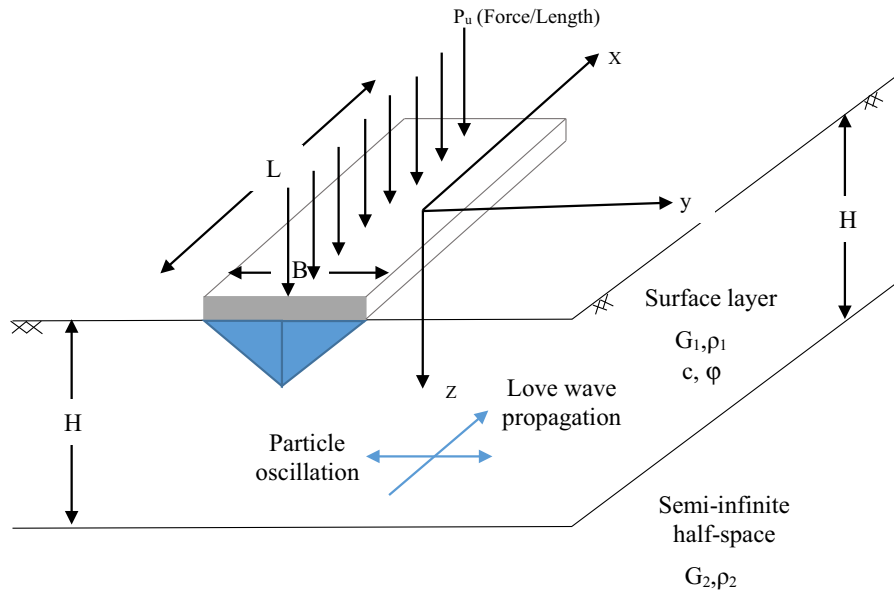


Fig. 2 Schematic illustration of the soil profile, shallow foundation with corresponding failure mechanism, and Love-wave propagation in the soil layer

the foundation width is assumed to lie in the particles’ transverse displacement direction.

According to Aki and Richards (1980) and Kramer (1996), while satisfying the traction-free surface assumption atop, the particle displacement can be found by:

$$v(x, z, t) = 2A_1 \cos \left[\omega \left(\frac{1}{v_{s1}^2} - \frac{1}{v_l^2} \right)^{1/2} z \right] e^{i(k_l x - \omega t)} \quad (2)$$

for $0 \leq z \leq H$

$$v(x, z, t) = 2A_1 \cos \left[\omega \left(\frac{1}{v_{s1}^2} - \frac{1}{v_l^2} \right)^{1/2} H \right] \exp \left[-\omega \left(\frac{1}{v_l^2} - \frac{1}{v_{s2}^2} \right)^{1/2} (z - H) \right] e^{i(k_l x - \omega t)} \quad (3)$$

for $z \geq H$

where v_{si} and v_l are the shear wave velocity in each layer ($i = 1, 2$) and Love wave velocity, respectively. As seen from Eqs. (2) and (3), the variation of the particle displacement amplitude of the Love wave with depth is harmonic and exponential for the surface layer and the half-space, respectively, decaying

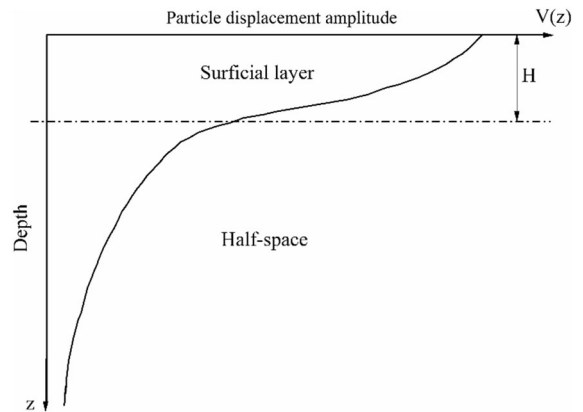


Fig. 3 Variation of the particle displacement amplitude with depth

readily by getting away from the surface as shown schematically in Fig. 3. Surface waves such as the Love wave, decay more slowly with distance than body waves do. Therefore, the effect of the surface waves is more eminent in comparison to the body waves in structures and superstructures afar. Hence, Love waves could be arguably the most destructive waves in areas that are far away from the focus of an earthquake. The Love wave velocity is admitted to be dependent on the excitation frequency, the surface layer thickness, and the shear moduli of both layers as

well as the shear wave velocities of each layer as shown in Eq. (4a). It is observed that the Love waves propagate at higher velocities with low frequencies which is limited to shear wave velocity of the stiffer underlying half-space. By increasing the excitation frequency, the Love waves are more inclined to propagate with the shear wave velocity of the softer surface layer, i.e. $v_{s1} < v_l < v_{s2}$.

$$\tan \left[\omega H \left(\frac{1}{v_{s1}^2} - \frac{1}{v_l^2} \right) 1/2 \right] = \frac{G_2}{G_1} \frac{\sqrt{\frac{1}{v_l^2} - \frac{1}{v_{s2}^2}}}{\sqrt{\frac{1}{v_{s1}^2} - \frac{1}{v_l^2}}} \tag{4a}$$

In principle, the Love wave velocity can be found both graphically and numerically for given values of frequency, surficial layer thickness, shear modulus ratio, and shear wave velocities of the surficial layer and semi-infinite half-space. In the graphical scheme of analysis, a new variable (X) was defined, and the Love wave velocity equation was re-written in the following form of Eq. (4b).

$$\tan[\omega X] = \frac{G_2 \sqrt{\frac{H^2}{v_l^2} - \frac{H^2}{v_{s2}^2}}}{G_1 X} \tag{4b}$$

where

$$X = H \sqrt{\frac{1}{v_{s1}^2} - \frac{1}{v_l^2}}$$

It is worth noting that, as the Love wave velocity is always more than the shear wave velocity of the surficial layer, the X variable is always positive. In order to find the Love wave velocity, the left- and right-hand sides of Eq. (4b) were sketched simultaneously. For a particular value of ω and a different value of X , the left-hand side (LHS) of Eq. (4b) could vary from $-\infty$ to $+\infty$, while the right-hand side (RHS) of Eq. (4b) is always positive within the interval of interest. Each intersection between the left-hand side and the right-hand side with respect to the constraint of $v_{s1} < v_l < v_{s2}$ corresponds to a real value of v_l . For real values of v_l boundary conditions are satisfied for the given value of ω . Another worth mentioning point is that there are several possible solutions (called modes) for a given value of X which are dependent on the ω values. The lowest Love wave velocity

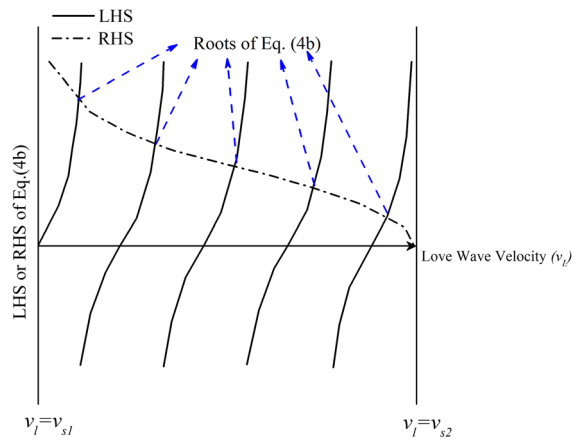


Fig. 4 Variation of the Love wave velocity with frequency

corresponds to the fundamental mode while the other solutions are called overtones. Figure 4 shows schematically the Love wave solution by the graphical approach (Verruijt 2010).

Another approach which is followed in this study is the numerical scheme of analysis. For this purpose, by factorizing the Love wave velocity from the right and left-hand sides of Eq. (4a), substituting Eqs. (5)–(7) in Eq. (4a), and after simplification, the Love wave velocity equation can be expressed as Eq. (8).

$$k_l = \frac{\omega}{v_l} = \frac{2\pi}{\lambda} \tag{5}$$

$$\bar{c} = \frac{v_{s2}}{v_{s1}} \tag{6}$$

$$G_i = \rho v_{si}^2 \tag{7}$$

$$\begin{aligned} \tan \left(\frac{2\pi H}{\lambda} \sqrt{\left(\frac{v_l}{v_{s1}} \right)^2 - 1} \right) &= \tan \left(k_l H \sqrt{\left(\frac{v_l}{v_{s1}} \right)^2 - 1} \right) \\ &= \frac{\rho_2 \bar{c}^2}{\rho_1} \frac{\sqrt{1 - \frac{1}{\bar{c}^2} \left(\frac{v_l}{v_{s1}} \right)^2}}{\sqrt{\left(\frac{v_l}{v_{s1}} \right)^2 - 1}} \end{aligned} \tag{8}$$

where λ is the Love wavelength. Now for any arbitrary value of the dimensionless frequency of the Love wave ($k_l H$), shear waves velocity ratio (\bar{c}), and density ratio (ρ_2/ρ_1), the ratio of Love wave velocity to the shear wave velocity of the surficial layer (v_l/v_{s1}) can be yielded numerically. By applying this formulation, a

specific value can be found for the ratio of the Love wave velocity to the shear wave velocity of the surficial layer (v_l/v_{s1}) for fixed and particular values of the Love wave non-dimensional frequency ($k_l H$), the shear waves velocity ratio (\bar{c}), and the density ratio (ρ_2/ρ_1).

3 Problem Definition and Assumptions

This study aims to evaluate the effect of the Love wave propagation on the seismic bearing capacity of a shallow foundation which is shown in Fig. 5. A shallow strip footing of width B is placed at a depth of D_f over soil with the unit weight of γ and shear strength parameters friction angle, φ and cohesion, c , with an underlying bedrock stretching horizontally to infinity and located at a depth of H to the footing. An idealized uniform pressure is assumed to simulate the effect of the surcharge. Moreover, the resistive effect of the soil overlying the foundation top is neglected. Following the study of Richards et al. (1993, 1994), the efficiency of the Coulomb failure mechanism as a viable alternative to the general shear failure mechanism was proven by Ghosh (2008), Ghosh and Debnath (2017), Saha and Ghosh (2017), and Izadi et al. (2019a) in the case of calculation of seismic bearing capacity. The simplified Coulomb failure mechanism consists of an active wedge (ΔABC) directly beneath the foundation, a passive wedge

Fig. 5 Seismic Coulomb failure mechanism adopted in the current study

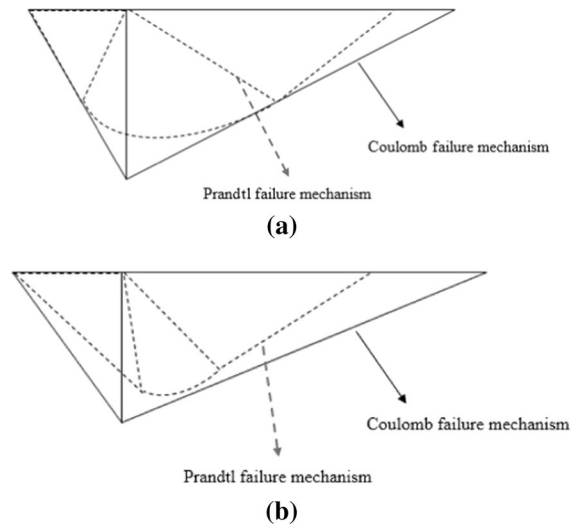
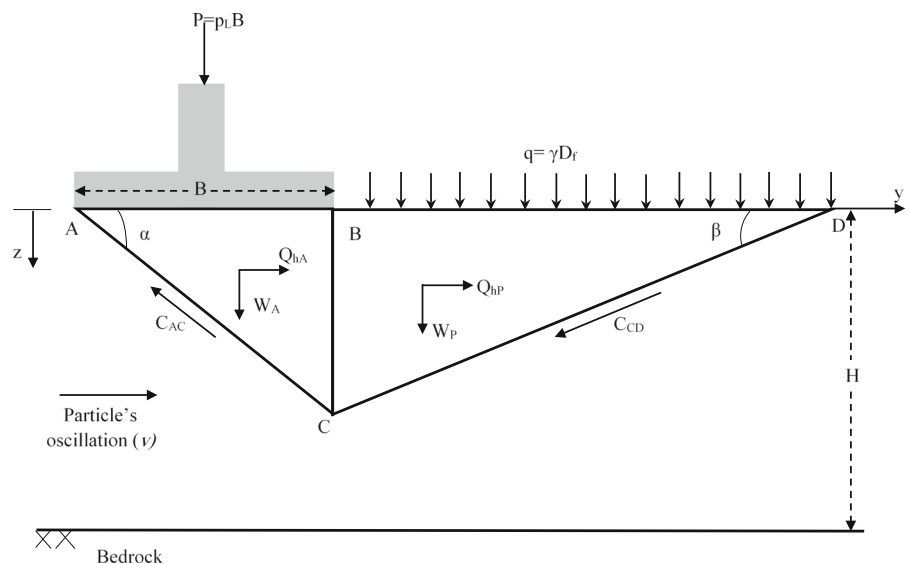


Fig. 6 Schematic representations of the slip lines; **a** static condition; and **b** seismic condition (Richards et al. 1994; Izadi et al. 2019a)

(ΔBCD) adjacent to the active wedge, and an interface wall between the active and passive zones (line BC) as shown in Fig. 5. In the simplified Coulomb failure mechanism, the transitional shear fan zone is not eliminated; instead, it is merged with the passive wedge due to asymmetric seismic loading condition as pointed out by Izadi et al. (2019a). This can be easily deduced by comparing different parts of Fig. 6. It is noteworthy that the implementation of the Prandtl failure mechanism and consequently the simplified Coulomb failure mechanism was widely proven to be

more accurate when the soil-foundation interface was perfectly rough. In the case of smooth soil-foundation interface, the Hill mechanism will be used to calculate bearing capacity of foundations (Fang 2013).

The borders of active and passive zones make the inclination angles of α and β with horizontal surface, respectively. P_A is the active thrust pushing the adjacent passive zone and P_P is the passive thrust, resisting the active wedge as shown in Fig. 7. The active and passive lateral earth pressures are equated to satisfy equilibrium conditions and should be found in a way that led to the more conservative ultimate load P . The soil shear strength parameters were adopted to be independent of the occurrence of an earthquake. No water table was considered and the critical failure mechanism is solely placed in the surficial layer which is schematically shown in Fig. 5.

In this study, the joint bearing capacity factors ($N_{\gamma eq}$) considering the simultaneous actions of all the contributors including soil cohesion, soil unit weight, and surcharge are calculated by limit equilibrium method. Despite the fact that individual consideration of the different contributors and their superposition

may lead to a more conservative solution in comparison to the simultaneous action of all the contributors as discussed by Jamshidi Chenari et al. (2018), a single failure mechanism will be invoked in the course of calculations. The formulation of modified pseudo-dynamic bearing capacity as introduced by Ghosh and Kolathayar (2011), and Bellezza (2014, 2015) was extended for the case of the Love wave propagation. A parametric analysis was also conducted to evaluate the influence of the most effective parameters such as the soil internal friction angle (φ), the interface wall friction angle (δ), the earthquake coefficient of acceleration (k_h), and the Love wave non-dimensional frequency ($k_t H$).

4 Method of Analysis

The seismic bearing capacity formulation to capture the effect of the Love wave propagation was derived using the limit equilibrium method (LEM) associated with the two-wedge Coulomb failure mechanism. As stated earlier, the propagation of the Love wave solely induces horizontal particle motion in the direction perpendicular to the wave traveling course. In order to calculate the inertia forces induced by the seismic excitation, the seismic acceleration due to the Love wave-induced particle motion should be calculated. According to Eq. (2), the horizontal acceleration field for the Love wave can be written as Eq. (9).

$$\begin{aligned}
 a(x, z, t) &= \frac{\partial^2 v}{\partial t^2} \\
 &= -2A_1 \omega^2 \cos \left[\omega \left(\frac{1}{v_{s1}^2} - \frac{1}{v_l^2} \right)^{1/2} z \right] e^{i(k_t x - \omega t)}
 \end{aligned}
 \tag{9}$$

Assuming a thin element with the thickness of dz at depth z in the active wedge as shown in Fig. 7, the horizontal inertia force acting on the active wedge can be obtained through integration within the failure mechanism depth.

$$Q_{hA}(t) = \frac{k_h \gamma \left[\cos \left(k_t H \frac{B \tan \alpha}{H} \sqrt{\left(\frac{v_l}{v_{s1}} \right)^2 - 1} \right) - 1 \right] [\sin(\omega t - k_t L) - \sin(\omega t)]}{k_t^3 \tan \alpha \cos \left[k_t H \sqrt{\left(\frac{v_l}{v_{s1}} \right)^2 - 1} \right] \left(\left(\frac{v_l}{v_{s1}} \right)^2 - 1 \right)}
 \tag{10}$$

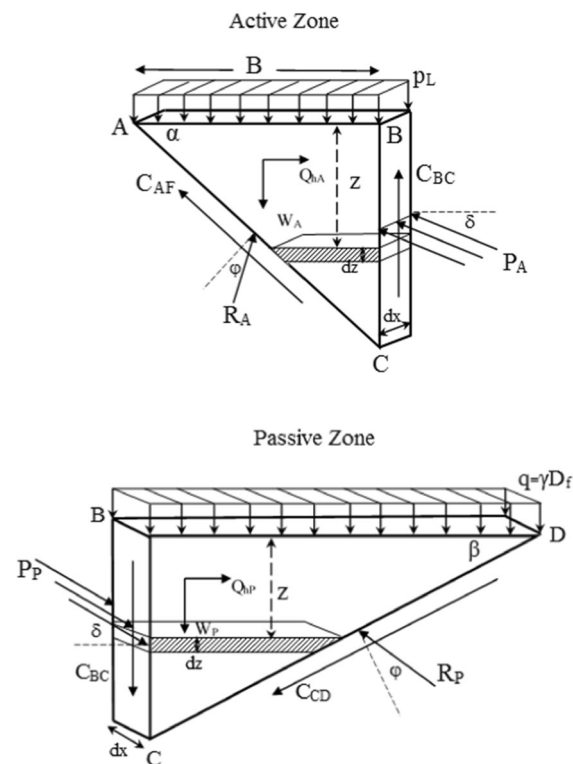


Fig. 7 Forces acting on the failure wedges

The total horizontal inertia force acting on the passive wedge can be written in the form of Eq. (11).

$$Q_{hp}(t) = \frac{k_h \gamma \left[\cos \left(k_t H \frac{B \tan \alpha}{H} \sqrt{\left(\frac{v_t}{v_{s1}} \right)^2 - 1} \right) - 1 \right] \left(1 + \frac{2D_f}{B \tan \alpha} \right) [\sin(\omega t - k_t L) - \sin(\omega t)]}{k_t^2 \tan \beta \cos \left[k_t H \sqrt{\left(\frac{v_t}{v_{s1}} \right)^2 - 1} \right] \left(\left(\frac{v_t}{v_{s1}} \right)^2 - 1 \right)} \tag{11}$$

Equilibrium conditions enforce the following equations on the forces applied to the active wedge:

$$\sum \vec{H} = 0 \tag{12}$$

$$P_A L \cos \delta = R_A L \sin(\alpha - \varphi) + Q_{hA} - cBL \tag{12a}$$

$$\uparrow \sum V = 0 \tag{13}$$

$$P_A L \sin \delta = -R_A L \cos(\alpha - \varphi) + W_A - 2cBL \tan \alpha + p_L BL \tag{13a}$$

where c is soil cohesion, R_A and P_A are the resultant force acting on the slip surfaces and the total seismic active resistance force, respectively, and W_A is the weight of the active wedge as follows:

$$W_A = \frac{1}{2} \gamma B^2 L \tan \alpha \tag{14}$$

After simplification and manipulation of Eqs. (12) and (13), the active force (P_A) can be found as Eq. (15):

$$P_A = \frac{Q_{hA} \cos(\alpha - \varphi)}{L \cos(\alpha - \varphi - \delta)} + \frac{W_A \sin(\alpha - \varphi)}{L \cos(\alpha - \varphi - \delta)} + p_L B \frac{\sin(\alpha - \varphi)}{\cos(\alpha - \varphi - \delta)} - cB \left\{ \frac{\cos(\alpha - \varphi)}{\cos(\alpha - \varphi - \delta)} + \frac{2 \tan \alpha \sin(\alpha - \varphi)}{\cos(\alpha - \varphi - \delta)} \right\} \tag{15}$$

Similarly, equilibrium conditions enforce the following equations on the forces applied to the passive wedge:

$$\sum \vec{H} = 0 \tag{16}$$

$$P_p L \cos \delta = R_p L \sin(\beta + \varphi) - Q_{hp} + cBL \frac{\tan \alpha}{\tan \beta} \tag{16a}$$

$$\uparrow \sum V = 0 \tag{17}$$

$$P_p L \sin \delta = R_p L \cos(\beta + \varphi) - W_p - 2cBL \tan \alpha \tag{17a}$$

where W_p is the weight of the passive wedge defined as

$$W_p = \frac{\gamma_e B^2 L \tan^2 \alpha}{2 \tan \beta} \tag{18}$$

After simplification and manipulation of Eqs. (16) and (17), the total passive force (P_p) is obtained as:

$$P_p = -\frac{Q_{hp} \cos(\beta + \varphi)}{L \cos(\delta + \beta + \varphi)} + \frac{W_p \sin(\beta + \varphi)}{L \cos(\delta + \beta + \varphi)} + cB \left\{ \frac{\tan \alpha \cos(\beta + \varphi)}{\tan \beta \cos(\delta + \beta + \varphi)} + \frac{2 \tan \alpha \sin(\beta + \varphi)}{\cos(\delta + \beta + \varphi)} \right\} \tag{19}$$

As previously mentioned, P_p and P_A are equated to satisfy the equilibrium condition. Therefore, the ultimate limit load of P_L can be found:

$$p_L B \frac{\sin(\alpha - \varphi)}{\cos(\alpha - \varphi - \delta)} = -\frac{Q_{hA} \cos(\alpha - \varphi)}{L \cos(\alpha - \varphi - \delta)} - \frac{Q_{hp} \cos(\beta + \varphi)}{L \cos(\delta + \beta + \varphi)} + \frac{W_p \sin(\beta + \varphi)}{L \cos(\delta + \beta + \varphi)} - \frac{W_A \sin(\alpha - \varphi)}{L \cos(\alpha - \varphi - \delta)} + cB \left\{ \frac{\tan \alpha \cos(\beta + \varphi)}{\tan \beta \cos(\delta + \beta + \varphi)} + \frac{2 \tan \alpha \sin(\beta + \varphi)}{\cos(\delta + \beta + \varphi)} + \frac{\cos(\alpha - \varphi) + 2 \tan \alpha \sin(\alpha - \varphi)}{\cos(\alpha - \varphi - \delta)} \right\} \tag{20}$$

After simplifying and manipulation the Eq. (20), the equivalent seismic bearing capacity factor ($N_{\gamma eq} = 2p_L/\gamma B$) capturing the effect of the Love wave propagation can be found as Eq. (21).

The pseudo-dynamic bearing capacity factor depends on the soil properties (c, φ, γ), interface wall friction angle (δ), geometric parameters of the foundation (B, L, D_f), the corresponding failure mechanism (α, β) and the surficial soil layer (H), the seismic coefficient of acceleration (k_h), the dimensionless frequency of the Love wave ($k_t H$), the ratio of the Love wave velocity to the shear wave velocity of the surficial layer (v_t/v_{s1}), the dimensionless wavelength ratios ($B/\lambda, L/\lambda$) and the dimensionless time (t/T). Note

$$\begin{aligned}
 N_{\gamma_{eq}} = & \left[\frac{\sin(\beta + \varphi) \cos(\alpha - \varphi - \delta) \tan^2 \alpha}{\sin(\alpha - \varphi) \cos(\delta + \beta + \varphi) \tan \beta} \left(1 + \frac{2D_f}{B \tan \alpha} \right) - \tan \alpha \right] \\
 & - \frac{\left[2k_h \left[\cos \left(k_l H \frac{B \tan \alpha}{H} \sqrt{\left(\frac{v_l}{v_{s1}} \right)^2 - 1} \right) - 1 \right] \left[\sin \left(2\pi \left(\frac{t}{T} - \frac{t}{\lambda} \right) \right) - \sin \left(\frac{2\pi t}{T} \right) \right] \right]}{\left(\frac{2\pi B}{\lambda} \right)^2 \left(\frac{2\pi L}{\lambda} \right) \tan \alpha \cos \left[k_l H \sqrt{\left(\frac{v_l}{v_{s1}} \right)^2 - 1} \right] \left(\left(\frac{v_l}{v_{s1}} \right)^2 - 1 \right) \tan(\alpha - \varphi)} \\
 & - \frac{\left[2k_h \left[\cos \left(k_l H \frac{B \tan \alpha}{H} \sqrt{\left(\frac{v_l}{v_{s1}} \right)^2 - 1} \right) - 1 \right] \left(1 + \frac{2D_f}{B \tan \alpha} \right) \left[\sin \left(2\pi \left(\frac{t}{T} - \frac{t}{\lambda} \right) \right) - \sin \left(\frac{2\pi t}{T} \right) \right] \right]}{\left(\frac{2\pi B}{\lambda} \right)^2 \left(\frac{2\pi L}{\lambda} \right) \tan \beta \cos \left[k_l H \sqrt{\left(\frac{v_l}{v_{s1}} \right)^2 - 1} \right] \left(\left(\frac{v_l}{v_{s1}} \right)^2 - 1 \right)} \left(\frac{\cos(\beta + \varphi) \cos(\alpha - \varphi - \delta)}{\sin(\alpha - \varphi) \cos(\delta + \beta + \varphi)} \right) \\
 & + \frac{2c \cos(\alpha - \varphi - \delta)}{\gamma B \sin(\alpha - \varphi)} \left\{ \begin{aligned} & \frac{\tan \alpha \cos(\beta + \varphi)}{\tan \beta \cos(\delta + \beta + \varphi)} + \frac{2 \tan \alpha \sin(\beta + \varphi)}{\cos(\delta + \beta + \varphi)} \\ & + \frac{\cos(\alpha - \varphi) + 2 \tan \alpha \sin(\alpha - \varphi)}{\cos(\alpha - \varphi - \delta)} \end{aligned} \right\}
 \end{aligned} \tag{21}$$

that the ratio of the Love wave velocity to the shear wave velocity of the surficial layer (v_l/v_{s1}) is also a function of the dimensionless frequency of the Love wave ($k_l H$), the shear wave velocity ratio (\bar{c}), and the density ratio (ρ_2/ρ_1) as stated before. Steedman and Zeng (1990) stated that for most of the earthquakes, the dominant earthquake periods vary between 0.2 and 0.5 s and the value of H/TV_s has the range of 0.2–0.5 while Ghosh (2008) and Saha and Ghosh (2015) proposed a wider range of 0.3–0.6 for H/TV_s . As the Love wave velocity is higher than the shear wave velocity of the surficial layer, the proposed range of Steedman and Zeng (1990) is deemed more appropriate.

5 Result and discussion

The results are reported for practical ranges of parameters as $\varphi = 20\text{--}40^\circ$, $\delta/\varphi = 0\text{--}1$, $2c/\gamma B = 0\text{--}0.5$, $D_f/B = 0.25\text{--}1$, $k_h = 0\text{--}0.3$, and different ratios of the Love wave velocity to the shear wave velocity of the surficial layer (v_l/v_{s1}). The solutions were found through an optimization process with the best combinations of geometry variables and time parameter which led to the least limit load. The objective function of this study (joint bearing capacity factor), input parameters of the Love wave velocity and the constraints of the objective function are as follow:

Input parameter of the Love wave velocity, i.e. Equation (8):

$$\frac{H}{\lambda}, \bar{c}, \frac{\rho_2}{\rho_1}$$

The output of Eq. (8):

$$\frac{v_l}{v_{s1}}$$

Input parameters of the bearing capacity factor, i.e. Equation (21):

$$\frac{c}{\gamma B}, \varphi, \delta, k_l H, \frac{H}{\lambda}, \frac{D_f}{B}, \frac{B}{L, H}, k_h, \frac{v_l}{v_{s1}}$$

where

$$N_{\gamma_{eq}} = f \left(\frac{c}{\gamma B}, \varphi, \alpha, \beta, \delta, k_l H, \frac{H}{\lambda}, \frac{D_f}{B}, \frac{B}{L, H}, k_h, \frac{t}{T}, \frac{v_l}{v_s}, \bar{c}, \frac{\rho_2}{\rho_1} \right) \tag{22}$$

Minimize $N_{\gamma_{eq}}$

Variable parameters: $\alpha, \beta, \frac{t}{T}$

Subjected to: $0^\circ \leq \alpha \leq 90^\circ$

$0^\circ \leq \beta \leq 90^\circ$

$N_{\gamma_{eq}} \geq 0$

The results of equivalent static bearing capacity factors were reported in Table 1. For the sake of

Table 1 Static bearing capacity factor ($N_{\gamma_{eq}}$)

$H/B = L/B = 10, \bar{c}=5, \rho_2/\rho_1 = 1.5$

δ	$2c/\gamma B$	$\phi = 20^\circ$				$\phi = 30^\circ$				$\phi = 40^\circ$			
		D_f/B				D_f/B				D_f/B			
		0.25	0.5	0.75	1	0.25	0.5	0.75	1	0.25	0.5	0.75	1
0	0	5.45	7.72	9.93	12.10	15.38	20.32	25.13	29.87	45.65	57.26	68.60	79.78
	0.25	8.84	11.04	13.22	15.37	20.90	25.72	30.46	35.16	55.34	66.74	77.96	89.06
	0.5	12.11	14.28	16.44	18.59	26.25	31.01	35.71	40.38	64.79	76.07	87.20	98.24
$\phi/2$	0	7.66	10.86	13.97	17.03	27.61	36.56	45.30	53.91	123.33	155.31	186.64	217.56
	0.25	11.85	14.94	18.00	21.03	35.98	44.73	53.36	61.90	144.65	176.17	207.21	237.94
	0.5	15.91	18.96	21.99	25.00	44.15	52.79	61.34	69.84	165.62	196.81	227.64	258.21
ϕ	0	10.61	15.05	19.38	23.65	55.45	73.69	91.53	109.15	–	–	–	–
	0.25	15.99	20.29	24.55	28.78	70.84	88.72	106.37	123.86	–	–	–	–
	0.5	21.20	25.44	29.66	33.87	85.91	103.58	121.09	138.49	–	–	–	–

validation of the computation procedure, a comparison was made between the results of the current study and Saha and Ghosh (2017). It should be noted that in the scarcity of any solution for pseudo-dynamic bearing capacity of shallow foundations with consideration of the effect of the Love wave on seismic bearing capacity, only the static bearing capacity factors were comparable to validate the results of the current findings. It is worth mentioning that the dimensionless

H/B and L/B ratios were maintained at 10, shear waves velocity ratio was assumed $\bar{c}=5$ and density ratio of $\rho_2/\rho_1 = 1.5$ was selected to find the ratio of the Love wave velocity to the shear wave velocity of the surficial layer (Fig. 8).

The simultaneous actions of all contributors including, $\phi, \delta/\phi, 2c/\gamma B, D_f/B,$ and k_1H on the equivalent bearing capacity factors of shallow foundations are presented for different earthquake coefficients of

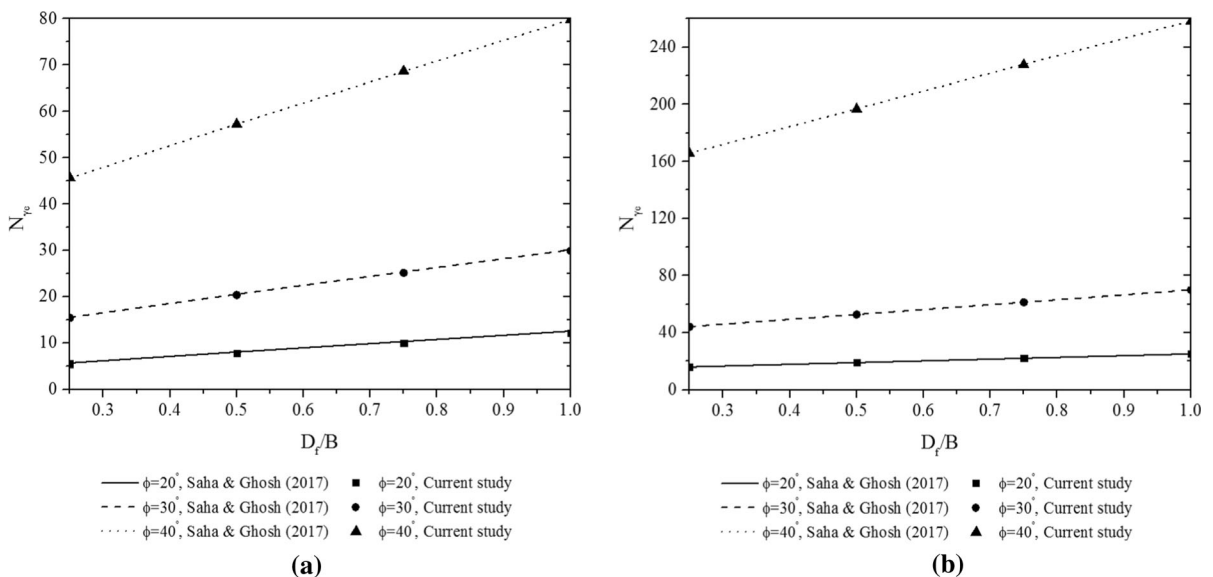


Fig. 8 Validation of the equivalent bearing capacity factor with Saha and Ghosh (2017); **a** $\delta = 0, 2c/\gamma B = 0$; and **b** $\delta = \phi/2, 2c/\gamma B = 0.5$

Table 2 Equivalent seismic bearing capacity factor ($N_{\gamma_{eq}}$) for $k_h = 0.1$

$H/B = L/B = 10, \bar{c} = 5, \rho_2/\rho_1 = 1.5$

		$k_l H = 3$				$k_l H = 5$				$k_l H = 10$				
		D_f/B												
δ	$2c/\gamma B$	0.25	0.5	0.75	1	0.25	0.5	0.75	1	0.25	0.5	0.75	1	
$\varphi = 20^\circ$	0	0	4.75	6.88	8.94	10.97	5.30	7.55	9.74	11.89	5.39	7.67	9.89	12.06
		0.25	8.08	10.45	12.16	14.17	8.69	10.87	13.02	15.15	8.80	11.01	13.18	15.34
		0.5	11.32	13.34	15.35	17.34	11.96	14.11	16.24	18.37	12.08	14.25	16.41	18.56
	$\varphi/2$	0	6.87	9.89	12.81	15.69	7.49	10.65	13.73	16.76	7.58	10.78	13.89	16.96
		0.25	11.02	13.93	16.80	19.65	11.68	14.74	17.76	20.76	11.79	14.88	17.94	20.97
		0.5	15.05	17.92	20.76	23.59	15.74	18.75	21.75	24.73	15.86	18.90	21.93	24.94
	φ	0	9.73	13.95	18.05	22.09	10.42	14.81	19.10	23.33	10.51	14.94	19.27	23.53
		0.25	15.07	19.16	23.19	27.19	15.79	20.05	24.27	28.45	15.91	20.20	24.45	28.67
		0.5	20.26	24.29	28.28	32.26	21.00	25.21	29.38	33.54	21.13	25.36	29.58	33.77
$\varphi = 30^\circ$	0	0	14.33	19.09	23.72	28.27	15.20	20.12	24.91	29.63	15.37	20.31	25.13	29.87
		0.25	19.80	24.44	29.00	33.50	20.72	25.52	30.24	34.91	20.89	25.72	30.46	35.16
		0.5	25.12	29.69	34.21	38.69	26.07	30.80	35.49	40.14	26.24	31.00	35.71	40.38
	$\varphi/2$	0	26.30	34.99	43.46	51.80	27.36	36.28	44.98	53.56	27.57	36.53	45.28	53.90
		0.25	34.64	43.12	51.48	59.75	35.74	44.45	53.04	61.55	35.95	44.71	53.34	61.89
		0.5	42.78	51.15	59.43	67.65	43.91	52.51	61.06	69.49	44.13	52.77	61.33	69.83
	φ	0	53.77	71.59	89.02	106.22	55.13	73.30	91.08	108.63	55.39	73.63	91.48	109.10
		0.25	69.12	86.59	103.82	120.90	70.52	88.34	105.92	123.35	70.79	88.68	106.32	123.82
		0.5	84.16	101.42	118.52	135.51	85.59	103.20	120.64	137.98	85.87	103.54	121.06	138.46
$\varphi = 40^\circ$	0	0	44.08	55.48	66.60	77.56	45.45	57.05	68.39	79.56	45.64	57.25	68.59	79.75
		0.25	53.74	64.93	75.93	86.80	55.15	66.55	77.76	88.84	55.33	66.73	77.94	89.03
		0.5	63.17	74.23	85.14	95.95	64.57	75.83	86.95	97.97	64.78	76.05	87.18	98.20
	$\varphi/2$	0	121.04	152.60	183.50	214.00	122.94	154.88	186.17	217.04	123.33	155.31	186.63	217.54
		0.25	142.34	173.43	204.05	234.35	144.27	175.75	206.75	237.43	144.65	176.16	207.19	237.91
		0.5	163.28	194.05	224.45	254.60	165.25	196.40	227.18	257.72	165.62	196.80	227.62	258.19
	φ	0	–	–	–	–	–	–	–	–	–	–	–	–
		0.25	–	–	–	–	–	–	–	–	–	–	–	–
		0.5	–	–	–	–	–	–	–	–	–	–	–	–

accelerations in Tables 2, 3 and 4. In the following sections, the impact of each effective parameter is elaborated and discussed.

5.1 Soil Friction Angle Impact

Superimposed on Fig. 9 are the results of equivalent seismic bearing capacity factors for different Love wave acceleration coefficients and $\varphi = 20\text{--}40^\circ$. In general, it is observed that the excitation induced by the Love wave propagation gives rise to a reduction in

the seismic bearing capacity of shallow foundations. As expected, the soil with a higher internal friction angle has a higher range of the pseudo-dynamic bearing capacity factor. This is obvious as the bearing capacity coefficient N_γ varies exponentially with the internal friction angle. It is further observed that almost for all frequency levels the seismic bearing capacity decreases with the Love wave amplitude; however, when the frequency rises due to the reduced wavelength, out-of-plane inertia forces along the footing length counteract in integral form. This means

Table 3 Equivalent seismic bearing capacity factor ($N_{\gamma_{eq}}$) for $k_h = 0.2$

$H/B = L/B = 10, \bar{c}=5, \rho_2/\rho_1 = 1.5$

		$k_l H = 3$				$k_l H = 5$				$k_l H = 10$				
		D_f/B												
δ	$2c/\gamma B$	0.25	0.5	0.75	1	0.25	0.5	0.75	1	0.25	0.5	0.75	1	
$\varphi = 20^\circ$	0	0	4.02	5.98	7.86	9.69	5.08	7.30	9.45	11.57	5.33	7.62	9.84	12.02
		0.25	7.29	9.17	11.02	1.85	8.46	10.61	12.72	14.82	8.76	10.97	13.14	15.30
		0.5	10.49	12.35	14.18	15.99	11.73	13.84	15.94	18.03	12.04	14.22	16.38	18.53
	$\varphi/2$	0	6.06	8.87	11.57	14.23	7.23	10.35	13.38	16.36	7.50	10.70	13.81	16.88
		0.25	10.16	12.87	15.53	18.16	11.42	14.43	17.40	20.36	11.73	14.82	17.87	20.90
		0.5	14.17	16.83	19.47	22.08	15.47	18.44	21.39	24.32	15.81	18.85	21.87	24.88
	φ	0	8.82	12.79	16.64	20.42	10.12	14.45	18.67	22.84	10.41	14.84	19.15	23.42
		0.25	14.13	17.98	21.76	25.51	15.49	19.69	23.84	27.96	15.82	20.11	24.35	28.57
		0.5	19.30	23.09	26.84	30.57	20.71	24.84	28.96	33.05	21.06	25.28	29.49	33.67
$\varphi = 30^\circ$	0	0	13.26	17.83	22.27	26.62	14.92	19.81	24.57	29.26	15.35	20.30	25.12	29.86
		0.25	18.69	23.13	27.49	31.80	20.44	25.21	29.90	34.55	20.89	25.71	30.46	35.15
		0.5	23.97	28.34	32.66	36.95	25.80	30.50	35.15	39.77	26.24	31.00	35.71	40.38
	$\varphi/2$	0	24.98	33.39	41.57	49.63	27.00	35.86	44.51	53.03	27.53	36.50	45.25	53.88
		0.25	33.28	41.49	49.56	57.55	35.38	44.04	52.57	61.03	35.93	44.69	53.33	61.88
		0.5	41.40	49.49	57.49	65.43	43.56	52.10	60.56	68.96	44.11	52.76	61.32	69.82
	φ	0	52.06	69.46	86.46	103.23	54.64	72.71	90.39	107.86	55.32	73.57	91.43	109.05
		0.25	67.38	84.44	101.24	117.89	70.03	87.76	105.24	122.57	70.74	88.63	106.28	123.78
		0.5	82.40	99.24	115.92	132.48	85.11	102.62	119.97	137.21	85.83	103.51	121.02	138.43
$\varphi = 40^\circ$	0	0	42.50	53.68	64.58	75.31	45.15	56.75	68.07	79.22	45.64	57.24	68.57	79.73
		0.25	52.13	63.10	73.87	84.51	54.87	66.25	77.44	88.51	55.32	66.71	77.92	88.99
		0.5	61.54	72.37	83.05	93.64	64.34	75.559	86.70	97.71	64.77	76.03	87.15	98.17
	$\varphi/2$	0	118.75	149.88	180.35	210.41	122.55	154.45	185.69	216.53	123.33	155.30	186.62	217.52
		0.25	140.01	170.68	200.86	230.74	143.89	175.32	206.28	236.93	144.64	176.15	207.18	237.89
		0.5	160.93	191.27	221.24	250.97	164.89	195.99	226.73	257.22	165.61	196.79	227.60	258.16
	φ	0	–	–	–	–	–	–	–	–	–	–	–	–
		0.25	–	–	–	–	–	–	–	–	–	–	–	–
		0.5	–	–	–	–	–	–	–	–	–	–	–	–

that the seismic bearing capacity does not undergo changes with the Love wave propagation substantiated in form of the horizontal bearing capacity lines in Fig. 9 and also almost similar numbers corresponding to $k_l H = 10$ among Tables 2, 3 and 4.

5.2 Interface Wall Friction Angle Impact

It can be seen from Fig. 10 that the equivalent seismic bearing capacity factor of a shallow foundation increases significantly with an increase of the wall

interface friction angle. The values of the seismic bearing capacity factor of $\delta = \varphi/2$ and $\delta = \varphi$ are relatively 2 and 4 times the seismic bearing capacity factor of the case when $\delta = 0$, respectively. Similar to the impact of the soil internal friction angle, the effect of the Love wave excitation is more eminent for a lower frequency.

Table 4 Equivalent seismic bearing capacity factor ($N_{\gamma_{eq}}$) for $k_h = 0.3$

$H/B = L/B = 10, \bar{c}=5, \rho_2/\rho_1 = 1.5$

		$k_l H = 3$				$k_l H = 5$				$k_l H = 10$				
		D_f/B												
δ	$2c/\gamma B$	0.25	0.5	0.75	1	0.25	0.5	0.75	1	0.25	0.5	0.75	1	
$\varphi = 20^\circ$	0	0	3.22	4.91	6.52	8.10	4.89	7.09	9.21	11.30	5.26	7.56	9.79	11.98
		0.25	6.43	8.10	9.72	11.31	8.27	10.39	12.47	14.54	8.71	10.92	13.10	15.26
		0.5	9.61	11.26	12.88	14.48	11.53	13.62	15.69	17.75	12.01	14.19	16.35	18.50
	$\varphi/2$	0	5.19	7.73	10.17	12.55	7.01	10.09	13.08	16.02	7.41	10.62	13.73	16.79
		0.25	9.26	11.73	14.14	16.52	11.20	14.17	17.10	20.01	11.66	14.75	17.80	20.83
		0.5	13.25	15.68	18.08	20.46	15.26	18.18	21.08	23.97	15.75	18.79	21.81	24.82
	φ	0	7.87	11.56	15.10	18.58	9.87	14.15	18.32	22.42	10.30	14.72	19.04	23.29
		0.25	13.16	16.74	20.24	23.70	15.25	19.39	23.49	27.55	15.73	20.02	24.25	28.46
		0.5	18.31	21.84	25.33	28.78	20.46	24.54	28.60	32.64	20.98	25.20	29.40	33.57
$\varphi = 30^\circ$	0	0	12.16	16.53	20.76	24.90	14.68	19.55	24.29	28.95	15.33	20.29	29.98	29.86
		0.25	17.54	21.78	25.94	30.04	20.21	24.95	29.62	34.24	20.88	25.71	30.46	35.15
		0.5	22.79	26.96	31.08	35.15	25.57	30.25	34.87	39.46	26.23	31.00	35.71	40.38
	$\varphi/2$	0	23.63	31.75	39.64	47.40	26.69	35.51	44.11	52.59	27.49	36.47	45.23	53.86
		0.25	31.90	39.82	47.60	55.29	35.08	43.69	52.18	60.58	35.90	44.67	53.31	61.86
		0.5	40.00	47.80	55.51	63.15	43.26	51.76	60.17	68.52	44.10	52.74	61.31	69.81
	φ	0	50.33	67.30	83.86	100.19	54.23	72.22	89.82	107.20	55.26	73.51	91.37	109.01
		0.25	65.62	82.25	98.62	114.84	69.63	87.27	104.67	121.93	70.69	88.58	106.24	123.74
		0.5	80.61	97.03	113.28	129.41	84.71	102.14	119.41	136.57	85.79	103.47	120.98	138.39
$\varphi = 40^\circ$	0	0	40.90	51.86	62.53	73.03	44.90	56.49	67.80	78.94	45.63	57.23	68.55	79.70
		0.25	50.51	61.24	71.79	82.20	54.63	66.00	77.18	88.24	55.31	66.70	77.89	89.96
		0.5	59.90	70.49	80.95	91.30	64.12	75.35	86.44	97.44	64.75	76.01	87.12	98.13
	$\varphi/2$	0	116.43	147.13	177.16	206.79	122.15	154.01	185.21	216.01	123.33	155.30	186.60	217.50
		0.25	137.67	167.90	197.66	227.10	143.52	174.90	205.82	236.42	144.64	176.14	207.16	237.86
		0.5	158.57	188.47	218.02	247.31	164.52	195.57	226.27	256.72	165.60	196.77	227.58	258.13
	φ	0	–	–	–	–	–	–	–	–	–	–	–	–
		0.25	–	–	–	–	–	–	–	–	–	–	–	–
		0.5	–	–	–	–	–	–	–	–	–	–	–	–

5.3 Embedment Depth Impact

As illustrated in Fig. 11, the footings with higher embedment depth ratio have a higher range of surcharge and passive resistance. Consequently, these increases raise the limit load sustained by the footings.

5.4 Soil Cohesion Impact

Figure 12 demonstrates the variation of the equivalent seismic bearing capacity factor for different values of

the dimensionless cohesion factor. As the resisting forces acting on the slip surfaces of the assumed failure mechanism increase, the ultimate limit pressure and the equivalent bearing capacity factor increase, accordingly.

5.5 The Influence of the Love wavelength

The bearing capacity of shallow footings subjected to the Love wave propagations becomes more complicated if the wavelength is comparable with the

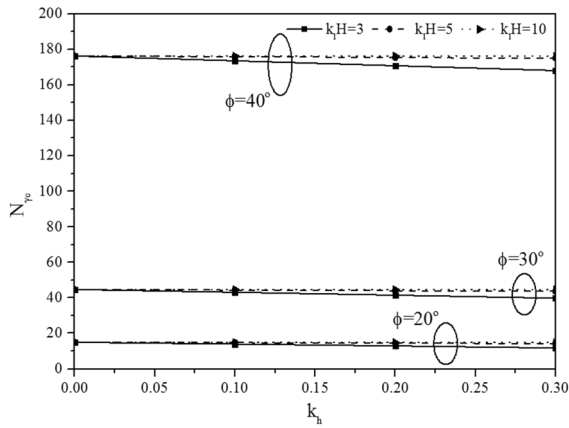


Fig. 9 Effect of the soil friction angle and Love wave acceleration coefficient on the equivalent seismic bearing capacity factor ($\delta = \varphi/2$, $2c/\gamma B = 0.25$, and $D_f/B = 0.5$)

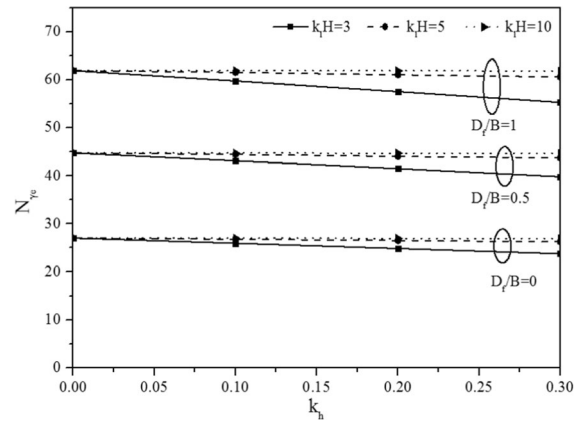


Fig. 11 Effect of the embedment depth ratio and Love wave acceleration coefficient on the equivalent seismic bearing capacity factor ($\varphi = 30^\circ$, $\delta = \varphi/2$, and $2c/\gamma B = 0.25$)

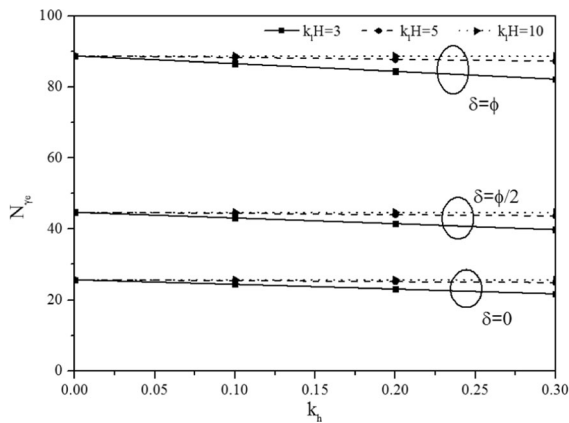


Fig. 10 Effect of the interface wall friction angle and Love wave acceleration coefficient on the equivalent seismic bearing capacity factor ($\varphi = 30^\circ$, $2c/\gamma B = 0.25$, and $D_f/B = 0.5$)

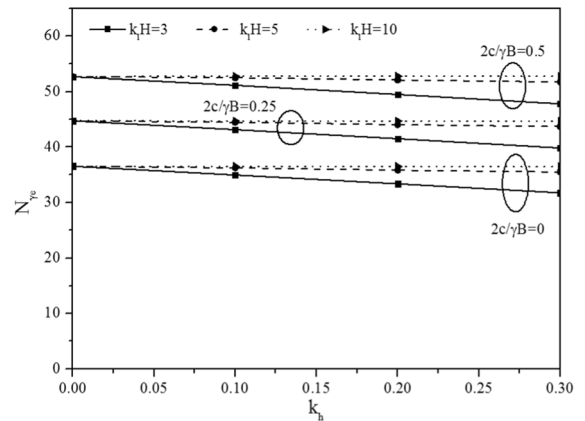


Fig. 12 Effect of the dimensionless cohesion ratio and Love wave acceleration coefficient on the equivalent seismic bearing capacity factor ($\varphi = 30^\circ$, $\delta = \varphi/2$, and $D_f/B = 0.5$)

foundation length. This means that the Love wave cycles along the footing length/width and exerts excitation transversely. Depending on the footing dimension along the propagation direction and the Love wavelength compared to it, the bearing capacity of the footing may be reduced or unaltered in some circumstances when the integral influence of the inertia forces becomes immaterial.

Incorporating this effect properly entails due adoption of a failure mechanism, which is relevant in three-dimension geometry. If plane strain condition is concerned, the most critical case is admittedly when the Love wave travels along the longer dimension. Even in such cases, the wavelength must be compared to the footing length. If the footing is infinitely long,

the Love wave-induced inertia forces in the out-of-plane direction harmonically fluctuate across the footing length and this presumably yields counteracted destabilizing force, hence the bearing capacity may remain unchanged.

Figure 13 demonstrates the results of the pseudo-dynamic bearing capacity factor by capturing the effect of the Love wavelength. As seen in this figure, the seismic bearing capacity factor reaches the static bearing capacity factor by increasing the value of the non-dimensional frequency $k_i H$. In fact, by increasing the Love wave frequency, its wavelength diminishes and therefore due to the periodic nature of the assumed wave front, many harmonic cycles of the back and forth particle displacement along the direction of the

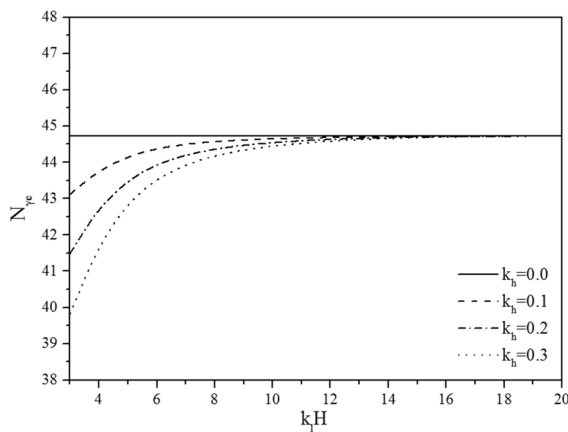


Fig. 13 Variation of the seismic bearing capacity factor with the Love wave frequency for different seismic coefficients of acceleration and $\varphi = 30^\circ$, $\delta = \varphi/2$, and $D_f/B = 0.5$, and $2c/\gamma B = 0.25$

wave propagation would have a neutralized influence. Hence, the net effect of the seismic excitation was negligible.

6 Summary and Conclusion

The equivalent seismic bearing capacity factor of shallow strip foundations in the presence of pseudo-dynamic earthquake accelerations induced by Love wave propagation has been evaluated by the limit equilibrium method (LEM). The equation of the particle displacement induced by the propagation of the Love wave was manipulated and the pseudo-dynamic bearing capacity formulation for shallow footings was extended to the three-dimensional Coulomb failure mechanism. The bearing capacity factor has been evaluated for the impacts of the most effective factors including geo-material properties, geometrical characteristics, and earthquake excitation frequency. The results of the equivalent bearing capacity of shallow foundations with three-dimensional Coulomb failure mechanism are in good agreement with those reported in the literature. Based on the results of this study, the equivalent seismic bearing capacity factor showed a direct relationship with soil strength parameters and non-dimensional frequency factor. The main conclusion of this study are:

1. An increase in shear strength parameters raises the resisting forces acting on the failure surface and consequently increases the ultimate limit load acting on the footing.
2. Love wave acceleration coefficient was found to have a decreasing impact on the bearing capacity of overlying shallow footing. The reduction of the limit load is more pronounced for higher values of the Love wave acceleration coefficient.
3. The influence of the Love wave propagation on the seismic bearing capacity of overlying shallow footings was found to be frequency-dependent. In other words, for lower non-dimensional frequency values, the bearing capacity of overlying shallow footings is expected to undergo reduction. Therefore, increasing the frequency of the Love wave, reflected in form of diminished wavelength, will in effect have less impact on bearing capacity reduction. This observation can be ascribed to the very fact that in the direction of wave propagation, depending on the Love wavelength relative to the footing length, phase shift will give rise to the out-of-plane displacement direction to shift in short distances; hence, yielding counter-acted unbalancing forces.
4. The results showed that the seismic bearing capacity factor increased gradually with the frequency of the Love wave up to the value of the static bearing capacity factor.
5. It was observed that augmentation of the soil cohesion and foundation embedment depth would hamper the destructing effects of Love wave interaction with the overlying shallow footings.
6. The practical significance of the findings of the current study lies in the importance of the surface wave propagation on performance of shallow foundations. Indeed, in areas located close to earthquake sources, or even sometime the locations far away from the earthquake source, it might happen the surface waves to adversely influence our infrastructures. Thus, provision of charts, similar to those presented in the current study, would pave the way towards better understanding of the seismic soil-structure interactions.

References

- Aki K, Richards P (1980) Quantitative seismology: theory and methods. Freeman and Company, San Francisco
- Askari F, Farzaneh O (2003) Upper-bound solution for seismic bearing capacity of shallow foundations near slopes. *Geotechnique* 53:697–702. <https://doi.org/10.1680/geot.2003.53.8.697>
- Bellezza I (2014) A new pseudo-dynamic approach for seismic active soil thrust. *Geotech Geol Eng* 32:561–576. <https://doi.org/10.1007/s10706-014-9734-y>
- Bellezza I (2015) Seismic active earth pressure on walls using a new pseudo-dynamic approach. *Geotech Geol Eng* 33:795–812. <https://doi.org/10.1007/s10706-015-9860-1>
- Budhu M, Al-Karni A (1993) Seismic bearing capacity of soils. *Geotechnique* 43:181–187. <https://doi.org/10.1680/geot.1993.43.1.181>
- Chakraborty D, Kumar J (2015) Seismic bearing capacity of shallow embedded foundations on a sloping ground surface. *Int J Geomech* 15:04014035. [https://doi.org/10.1061/\(asce\)gm.1943-5622.0000403](https://doi.org/10.1061/(asce)gm.1943-5622.0000403)
- Choudhury D, Nimbalkar S (2005) Seismic passive resistance by pseudo-dynamic method. *Geotechnique* 55:699–702. <https://doi.org/10.1680/geot.2005.55.9.699>
- Choudhury D, Rao KSS (2005) Seismic bearing capacity of shallow strip footings. *Geotech Geol Eng* 23:403–418. <https://doi.org/10.1007/s10706-004-9519-9>
- Fang HY (2013) Foundation engineering handbook. Springer Science & Business Media, New York
- Fathipour H, Safardoost Siahmazzi AH, Payan M, Veiskarami M, Jamshidi Chenari R (2021) Limit analysis of modified pseudo-dynamic lateral earth pressure in anisotropic medium using finite element and second-order cone programming. *Int J Geomech* 21:04020258. [https://doi.org/10.1061/\(asce\)gm.1943-5622.0001924](https://doi.org/10.1061/(asce)gm.1943-5622.0001924)
- Foroutan Kalourazi A, Izadi A, Jamshidi Chenari R (2019) Seismic bearing capacity of shallow strip foundations in the vicinity of slopes using the lower bound finite element method. *Soils Found* 59:1891–1905. <https://doi.org/10.1016/j.sandf.2019.08.014>
- Ghosh P (2008) Upper bound solutions of bearing capacity of strip footing by pseudo-dynamic approach. *Acta Geotech* 3:115–123. <https://doi.org/10.1007/s11440-008-0058-z>
- Ghosh P, Choudhury D (2011) Seismic bearing capacity factors for shallow strip footings by pseudo-dynamic approach. *Disaster Adv* 4:34–42
- Ghosh S, Debnath L (2017) Seismic bearing capacity of shallow strip footing with Coulomb failure mechanism using limit equilibrium method. *Geotech Geol Eng* 35:2647–2661. <https://doi.org/10.1007/s10706-017-0268-y>
- Ghosh P, Kolathayar S (2011) Seismic passive earth pressure behind non vertical wall with composite failure mechanism: pseudo-dynamic approach. *Geotech Geol Eng* 29:363–373. <https://doi.org/10.1007/s10706-010-9382-9>
- Haghsheno H, Jamshidi Chenari R, Javankhosdel S, Banirostam T (2020) Seismic bearing capacity of shallow strip footings on sand deposits with weak inter-layer. *Geotech Geol Eng* 38:6741–6754. <https://doi.org/10.1007/s10706-020-01466-4>
- Izadi A, Nazemi Sabet Soumehsaraei M, Jamshidi Chenari R, Ghorbani A (2019a) Pseudo-static bearing capacity of shallow foundations on heterogeneous marine deposits using limit equilibrium method. *Mar Georesour Geotechnol* 37:1163–1174. <https://doi.org/10.1080/1064119x.2018.1539535>
- Izadi A, Nazemi Sabet Soumehsaraei M, Jamshidi Chenari R, Moallemi S, Javankhosdel S (2019b) Spectral bearing capacity analysis of strip footings under pseudo-dynamic excitation. *Geomech Geoeng*. <https://doi.org/10.1080/17486025.2019.1670873>
- Izadi A, Foroutan Kalourazi A, Jamshidi Chenari R (2021) Effect of roughness on seismic bearing capacity of shallow foundations near slopes using the lower bound finite element method. *Int J Geomech*. [https://doi.org/10.1061/\(asce\)gm.1943-5622.0001935](https://doi.org/10.1061/(asce)gm.1943-5622.0001935)
- Jamshidi Chenari R, Izadi A, Nazemi Sabet Soumehsaraei M (2018) Discussion of “seismic bearing capacity of shallow strip footing with Coulomb failure mechanism using limit equilibrium method” by S. Ghosh, L. Debnath. December 2017, Volume 35, Issue 6, pp. 2647–2661. *Geotech Geol Eng* 36:4037–4040. <https://doi.org/10.1007/s10706-018-0497-8>
- Kramer SL (1996) Geotechnical earthquake engineering. In: Prentice–Hall international series in civil engineering and engineering mechanics. Prentice–Hall, Upper Saddle River, New Jersey
- Kumar J, Chakraborty D (2013) Seismic bearing capacity of foundations on cohesionless slopes. *J Geotech Geoenviron Eng* 139:1986–1993. [https://doi.org/10.1061/\(asce\)gt.1943-5606.0000909](https://doi.org/10.1061/(asce)gt.1943-5606.0000909)
- Kumar J, Kumar N (2003) Seismic bearing capacity of rough footings on slopes using limit equilibrium. *Geotechnique* 53:363–369. <https://doi.org/10.1680/geot.2003.53.3.363>
- Kumar J, Rao V (2002) Seismic bearing capacity factors for spread foundations. *Geotechnique* 52:79–88. <https://doi.org/10.1680/geot.2002.52.2.79>
- Kurup SS, Kolathayar S (2018) Seismic bearing capacity factor considering composite failure mechanism: pseudo-dynamic approach. *Int J Geotech Earthq Eng* 9:65–77. <https://doi.org/10.4018/ijgee.2018010104>
- Love A (1927) The mathematical theory of elasticity. University Press, Cambridge
- Meyerhof GG (1963) Some recent research on the bearing capacity of foundations. *Can Geotech J* 1:16–26. <https://doi.org/10.1139/t63-003>
- Nouzari MA, Jamshidi Chenari R, Payan M, Pishgar F (2021) Pseudo-static seismic bearing capacity of shallow foundations in unsaturated soils employing limit equilibrium method. *Geotech Geol Eng* 39:943–956. <https://doi.org/10.1007/s10706-020-01535-8>
- Pain A, Choudhury D, Bhattacharyya S (2015) Seismic stability of retaining wall–soil sliding interaction using modified pseudo-dynamic method. *Géotech Lett* 5:56–61. <https://doi.org/10.1680/geolett.14.00116>
- Pakdel P, Jamshidi Chenari R, Veiskarami M (2021) Seismic bearing capacity of shallow foundations rested on anisotropic deposits. *Int J Geotech Eng* 15:181–192. <https://doi.org/10.1080/19386362.2019.1655983>

- Paolucci R, Pecker A (1997) Seismic bearing capacity of shallow strip foundations on dry soils. *Soils Found* 37:95–105. https://doi.org/10.3208/sandf.37.3_95
- Richards R Jr, Elms DG, Budhu M (1993) Seismic bearing capacity and settlements of foundations. *J Geotech Eng* 119:662–674. [https://doi.org/10.1061/\(asce\)0733-9410\(1993\)119:4\(662\)](https://doi.org/10.1061/(asce)0733-9410(1993)119:4(662))
- Richards R Jr, Elms DG, Budhu M (1994) Closure to “seismic bearing capacity and settlements of foundations” by R. Richards Jr., DG Elms, and M. Budhu (April, 1993, Vol. 119, No. 4). *J Geotech Eng* 120:1637–1639. [https://doi.org/10.1061/\(asce\)0733-9410\(1994\)120:9\(1637\)](https://doi.org/10.1061/(asce)0733-9410(1994)120:9(1637))
- Saha A, Ghosh S (2015) Pseudo-dynamic analysis for bearing capacity of foundation resting on c - Φ soil. *Int J Geotech Eng* 9:379–387. <https://doi.org/10.1179/1939787914y.0000000081>
- Saha A, Ghosh S (2017) Modified pseudo-dynamic bearing capacity analysis of shallow strip footing considering total seismic wave. *Int J Geotech Eng*. <https://doi.org/10.1080/19386362.2017.1405542>
- Shearer PM (2009) *Introduction to seismology*. Cambridge University Press, Cambridge
- Soubra AH (1999) Upper-bound solutions for bearing capacity of foundations. *J Geotech Geoenviron Eng* 125:59–68. [https://doi.org/10.1061/\(asce\)1090-0241\(1999\)125:1\(59\)](https://doi.org/10.1061/(asce)1090-0241(1999)125:1(59))
- Steedman R, Zeng X (1990) The influence of phase on the calculation of pseudo-static earth pressure on a retaining wall. *Geotechnique* 40:103–112. <https://doi.org/10.1680/geot.1990.40.1.103>
- Verruijt A (2010) *An introduction to soil dynamics*. Springer Science & Business Media, Delft
- Yamamoto K (2010) Seismic bearing capacity of shallow foundations near slopes using the upper-bound method. *Int J Geotech Eng* 4:255–267. <https://doi.org/10.3328/ijge.2010.04.02.255-267>
- Zhou XP, Gu XB, Yu MH, Qian QH (2016) Seismic bearing capacity of shallow foundations resting on rock masses subjected to seismic loads. *KSCE J Civ Eng* 20:216–228. <https://doi.org/10.1007/s12205-015-0283-6>

Publisher's Note Springer Nature remains neutral with regard to jurisdictional claims in published maps and institutional affiliations.